energies

MDPI

Article

Parameter Identification for Proton Exchange Membrane Fuel Cell Using an Enhanced Puma Optimizer

Nawal Rai [1,*], Badreddine Kanouni [2], Abdelbaset Laib [3], Salah Necaibia [4], Saleh Al Dawsari [5,6,*] and Khalid Yahya [7,*]

1 Materials, Energy Systems Technology and Environment Laboratory, University of Ghardaia, Ghardaïa 47000, Algeria
2 Automatic and Intelligent Systems Department, University of Setif 1, Sétif 19000, Algeria; badreddine.kanouni@univ-setif.dz
3 Department of Automatic, Faculty of Electrical Engineering, University of Science and Technology Houari Boumediene, Algiers 16111, Algeria; laibabdelbasset42@gmail.com
4 Electromechanical Systems Laboratory (LSELM), Electrical Engineering Department, Faculty of Technology, Badji Mokhtar University, Annaba 23000, Algeria; salah.necaibia@univ-annaba.dz
5 School of Engineering, Cardiff University, Cardiff CF24 3AA, UK
6 Electrical Engineering Department, College of Engineering, Najran University, Najran P.O. Box 1988, Saudi Arabia
7 Department of Electrical & Electronics Engineering, Istanbul Gelisim University, Istanbul 34310, Turkey
* Correspondence: rainawel27@gmail.com (N.R.); aldawsarisa@cardiff.ac.uk (S.A.D.); hayahya@gelisim.edu.tr (K.Y.)

Abstract

Proton exchange membrane fuel cells (PEMFCs) represent a promising renewable energy technology that converts chemical energy from hydrogen and oxygen into electrical energy. Accurate mathematical modeling and precise parameter identification are essential for optimizing PEMFC performance and control. This study proposes a novel hybrid meta-heuristic algorithm, the mutated puma optimizer (Mu-PO), which integrates a mutation operator from differential evolution to enhance the exploration and exploitation capabilities of the conventional puma optimizer, enabling it to escape local minima and reach global optima in fewer iterations. A sum of squared error (SSE)-based objective function is formulated to minimize the discrepancy between estimated and experimental voltages. The proposed method identifies seven unknown parameters for three commercial PEMFC models (250 W, SR-12, and NedStack PS6), achieving SSE values of 0.6419, 1.0566, and 2.0791, respectively. Notably, Mu-PO attains these low SSE values in fewer than 50 iterations for all models, demonstrating rapid convergence. Comparative analysis using statistical indicators (minimum, mean, maximum, and standard deviation of SSE) confirms that Mu-PO outperforms well-established optimization algorithms in terms of convergence speed, stability, and accuracy. Furthermore, validation under dynamic operating conditions, including variations in pressure and temperature, demonstrates consistent and reliable parameter identification, highlighting the robustness and practical applicability of the proposed approach for PEMFC modeling and optimization.

Keywords: hydrogen; fuel cell; parameter extraction; hybrid meta-heuristic approach; stability; Amphlett model; convergence speed

Academic Editors: Xingwang Tang and Chuanyu Sun

Received: 31 January 2026
Revised: 23 February 2026
Accepted: 27 February 2026
Published: 2 March 2026

1. Introduction

Fuel cells (FCs) signify a notable progression in renewable energy technology owing to their longevity, efficiency, and environmentally sustainable characteristics. They are

progressively used in residential, commercial, and industrial sectors for diverse purposes, including stationary power generating, portable gadgets, and transportation. Fuel cells are classified according to the electrolyte used, with each category exhibiting distinct attributes concerning operating temperatures, power ranges, efficiency, and applicability [1]. FCs are divided into various types such as alkaline FCs [2], solid oxide FCs [3], phosphoric acid FCs [4], and proton exchange membrane fuel cells (PEMFCs) [5].

PEMFCs are distinguished by their straightforward design, increased power density, and low operating temperatures (30–100 °C). Nonetheless, the intrinsic complexity of PEMFCs presents difficulties in creating precise mathematical models that accurately represent their nonlinear characteristics and dynamic performance [6]. Accurate modeling is essential for performance evaluation, control, and optimization, but precise parameter identification remains a major challenge due to the limited information provided by manufacturers' datasheets [7]. The heat transport and catalytic coupling parameters of a PEMFC are explored in depth using a model with anisotropic electrode thermal conductivity. Electrochemical energy storage stands out above other technologies due to its remarkable efficiency in converting energy [8]. At different operating temperatures, the PEMFC's main heat source shifted from the electrochemical process heat generated in the cathode electrode to different molar concentration distributions of liquid water and oxygen on the electrode surface. This change was more pronounced in [9] than in other directions. The investigation of GDB durability in PEMFCs running under reverse current conditions is discussed in [10], using both experimental and computational methodologies.

PEMFC models can be broadly classified as mechanistic [11], empirical [12], or semi-empirical [13], with the polarization curve depicting the voltage–current relationship serving as a key performance indicator. The Amphlett model has become a well-recognized semi-empirical framework for evaluating the performance of PEMFCs under both steady-state and dynamic settings [14]. However, identifying the unknown parameters within this model remains a complex, multivariable optimization problem.

Traditional optimization techniques often struggle to accurately estimate these parameters due to the nonlinear nature of the polarization curves and the risk of becoming trapped in local optima [15]. As a result, more advanced optimization methods are needed to minimize the sum of squared errors (SSE) between measured and estimated data. In recent years, meta-heuristic algorithms have been applied to PEMFC parameter identification, as they offer powerful tools to navigate complex search spaces efficiently. For example, the slap swarm optimizer (SSO) was employed by El-Fergany to optimize the parameters of two commercial PEMFC stacks, NedStack PS6 and BCS-500 W PEM, demonstrating superior performance over conventional methods [16]. Similarly, Zhang et al. [17] modified the chaos owl search algorithm (COSA) to minimize the differences between the measured and estimated values. A PEMFC parameter estimation approach based on the bonobo optimizer (BO) was proposed by Sultan in [18] to address local minima challenges in PEMFC models. For PEMFC parameter estimation, the tree growth method [19] was modified to minimize SSE. The local optima in this algorithm continues to prevent it from achieving better precision. In [20], p-dimensional extremum seeking via a simplex tuning optimization method was proposed to identify the seven unknown parameters. A strategy based on the multi-verse optimizer (MVO) was presented by Fathy et al. [21] to estimate the unknown parameters of the PEMFC equivalent circuit operated under various circumstances. Many approaches that used meta-heuristic optimizers to estimate the PEMFC model's unknown parameters were examined in [22], such as the genetic algorithm (GA), which is complicated because of its many phases, including crossover, mutation, and selection. Additionally, it is dependent on the starting population. Because the fitness value

is computed repeatedly, some computing difficulties may exist. It has a low capacity for exploitation and the potential to prematurely converge on a less-than-ideal solution.

This restriction prompted researchers to use new GA modifications in order to arrive at the best answers. Artificial bee colony (ABC): Because fitness value is not taken into account while choosing a target, the neighbor of both employed and observer bees, it has a sluggish convergence speed. Backtracking search algorithm (BSA): It has moderate complexity and a quick rate of convergence. Although BSA has a sluggish computing speed, it can get global solutions. It needs a lot of RAM. Grey wolf optimization (GWO): The accuracy of the answers derived via GWO is lower. This approach has a slow rate of convergence and is inclined toward local optima.

Due to its straightforward structure, quick searching speed, and delayed convergence, the moth flame optimization algorithm (MFOA) causes the solution to get trapped in local optima. This approach prioritizes exploitation over exploration. Additional meta-heuristic techniques used in the literature to identify PEMFC parameters include the shark smell optimizer (SSO) [23], bird mating optimizer (BMO) [24], particle swarm optimization (PSO) [25], improved artificial ecosystem optimizer (IAEO) [26], differential evolution (DE) [27], and teaching learning-based optimization differential evolution algorithm (TL-BODE) [28]. Although these algorithms have demonstrated varying degrees of success, they often require further refinement to address the persistent challenges of local optima and slow convergence rates.

A multi-strategy tuna swarm optimization (MS-TSO) is proposed in reference [29] to estimate the parameters of PEMFC voltage models and to compare its efficacy with other optimization techniques, including differential evolution, the whale optimization algorithm, the slap swarm algorithm, particle swarm optimization, Harris hawk optimization, and the slime mold algorithm. To minimize the sum of squared errors between the estimated and measured data, the optimization method uses the undiscovered factors of the PEMFCs as choice variables.

The authors in [30] present a sophisticated method for accurate parameter estimation in PEMFC models. The enhanced walrus optimization (EWO) algorithm, along with Lévy flight exploration, addresses the intrinsic nonlinearity of PEMFC systems. The technique seeks to reduce the squared error between observed and simulated terminal voltage, therefore guaranteeing enhanced accuracy and resilience relative to conventional algorithms. The efficacy of the suggested model is confirmed by comparisons of theoretical simulations and experimental data. These challenges are widely reported in scientific literature and limit the effectiveness of existing optimization methods [19]. Most meta-heuristic algorithms initially prioritize extensive exploration to cover various areas of the search space. However, this approach often results in slower convergence, delaying identifying the optimal solution, even when a near-optimal solution is readily accessible. The second issue, local minima, could come up when an area of the search space is unsuitable due to the algorithm's inadequate search strength. These two issues lead us to suggest a novel meta-heuristic approach that will prevent local minima from forming and accelerating the convergence rate to the best-so-far solution.

This paper introduces a novel hybrid approach based on the mutated puma optimizer (Mu-PO), specifically developed to address optimization problems with large and complex search spaces. It is inspired by puma behavior and strategic hunting techniques [31]. The proposed algorithm offers a unique solution for parameter estimation in PEMFCs. This is the first application of the Mu-PO algorithm to address the parameter estimation challenge in PEMFCs.

Although the Mu-PO algorithm has been proposed and validated in extracting parameters from the mathematical models of several PEMFC stacks, the key contributions of this work are:

- A novel hybrid Mu-PO algorithm is especially designed to determine undefined parameters for PEMFCs, an area not previously explored in prior research.
- The algorithm is tested on three commercial PEMFCs: 250 W PEMFC, SR-12, and NedStack PS6, demonstrating superior convergence speed, stability, and accuracy compared to existing optimizers.
- Optimal parameter values obtained through Mu-PO are used to analyze the I-V polarization curve under varying temperatures and gas supply pressures.
- The sensitivity and reliability of the proposed algorithm are confirmed through a series of statistical tests.

The paper is structured as follows: Section 2 presents the mathematical formulation of PEMFCs, the objective function, and the proposed methodology. Section 3 details the hybrid Mu-PO algorithm in detail. Section 4 includes a series of statistical tests to evaluate the PO performance and presents numerical simulations of the PEMFC model under various steady-state conditions. Finally, Section 5 provides the conclusions.

2. PEMFC Model Description

2.1. PEMFC Mathematical Model

The Amphlett model is widely used in the literature to describe the behavior of proton exchange membrane fuel cells (PEMFCs). It establishes the relationship between the output voltage and the drawn current under steady-state operating conditions and can also be extended to account for transient situations. Due to its reliability and accuracy, it is considered one of the most representative semi-empirical models for PEMFC analysis. The overall output voltage of a single PEMFC cell (V_c) is expressed in Equation(1) [14].

$$V_c = E_{nrs} - V_{act} - V_{ohm} - V_{cons} \tag{1}$$

E_{nrs} is the voltage achieved on the cell's output connections when there is no load. The other variables are the activation (V_{act}) voltage, the ohmic voltage (V_{ohm}), and the concentration voltage (V_{cons}).

The cell output voltage typically ranges between 0.9 and 1.23 V, depending on the heating amount and regulating pressures. To achieve higher voltage levels, N_{fc} cells must be serially coupled, generating a PEMFC stack V_{st}, as described by Equation (2) [20,32]:

$$V_{st} = V_c \cdot N_{fc} \tag{2}$$

E_{nrs} is the voltage achieved on the cell's output connections when there is no-load operation and can be represented using the Equation (3) [20]:

$$E_{nrs} = 1.229 - 8.5 \times 10^{-4}\left(T_{fc} - 298.15\right) + 4.3085 \times 10^{-5} \times T_{fc} \times [ln(P_{H_2}) + 0.5\, ln(P_{O_2})] \tag{3}$$

P_{H_2} and P_{O_2} represents the hydrogen and oxygen pressure (Bar), provided in Equations (4) and (5):

$$P_{O_2} = Rh_c \cdot P_{H_2O}\left[\left(exp\left(\frac{4.192\left(I_{fc}/A\right)}{T_{fc}^{1.334}}\right) \times \frac{Rh_c P_{H_2O}}{P_c}\right)^{-1} - 1\right] \tag{4}$$

$$P_{H_2} = 0.5Rh_a \cdot P_{H_2O}\left[\left(exp\left(\frac{1.635\left(I_{fc}/A\right)}{T_{fc}^{1.334}}\right) \times \frac{Rh_a P_{H_2O}}{P_a}\right)^{-1} - 1\right] \quad (5)$$

where Rh_c and Rh_a denote the relative humidity related to the cathode and anode, respectively. I_{fc}, T_{fc}, A are the cell-produced current, operating temperature, and membrane projection area, respectively. P_{H_2O} is the water vapor saturation pressure, calculated using Equation (6):

$$P_{H_2O} = 2.95 \times 10^{-2}(T_{fc} - 273.15) - 9.18 \times 10^{-5}(T_{fc} - 273.15)^2 + 1.44 \times 10^{-7}(T_{fc} - 273.15)^3 - 2.18 \quad (6)$$

V_{act} is the activation voltage and represented as follows [33,34]:

$$V_{act} = \delta_1 + \delta_2 T_{fc} + \delta_3 T_{fc} ln\left(\frac{P_{O_2}}{5.08 \times 10^6 exp\left(\frac{-495}{T_{fc}}\right)}\right) + \delta_4 T_{fc} ln\left(I_{fc}\right) \quad (7)$$

$\delta_{1,2,3,4}$, are the semi-empirical parameters that require being identified.

The resistance facing the electrons flowing in the external circuit causes the V_{ohm} reaction in the PEMFC, which is determined using the following formula [32,35]:

$$V_{ohm} = I_{fc}(R_c + R_m) \quad (8)$$

where R_c stands for the connections' resistance, while the proton exchange membrane's equivalent resistance is denoted by R_m.

$$R_m = \frac{\rho_m l}{A} \quad (9)$$

ρ_m is the protons' encountered impedance, which can be determined using Equation (10), and the thickness of the membrane represented by l.

$$\rho_m = \frac{181.6\left[1 + 0.03\left(\frac{I_{fc}}{A}\right) + 0.062\left(\frac{T_{fc}}{303}\right)^2\left(\frac{I_{fc}}{A}\right)^2\right]}{\left[\lambda - 0.634 - 3\left(\frac{I_{fc}}{A}\right)\right] \times exp\left[4.18\left(\frac{T_{fc}-303}{T_{fc}}\right)\right]} \quad (10)$$

Equation (11) can be used to compute the concentration voltage (V_{cons}).

$$V_{cons} = -\beta\, ln\left(1 - \frac{J}{J_{max}}\right) \quad (11)$$

The parameter β needs to be determined, whereas J and J_{max} reflect the PEMFC's actual and maximum current density (A/cm^2).

It is observed that the PEMFC mathematical equation represented by (1)–(11) has a set of unknown parameters (δ_1, δ_2, δ_3, δ_4, λ, R_m, and β) that are not listed in the manufacturer's data. As a result, precisely identifying these parameters is seen to be the initial essential phase of developing the PEMFC model. In this paper, these parameters are extracted using the PO algorithm.

2.2. Problem Formulation and Objective Function

The preceding equations explained the PEMFC's essential operation. From there, it can be assumed that, within the constraints of every commercial FC stack's design, a set of the seven parameters (δ_1, δ_2, δ_3, δ_4, λ, R_m, and β) is experimentally modified to determine how the PEMFC operates. Figure 1 illustrates the PEMFC parameter estimation procedure.

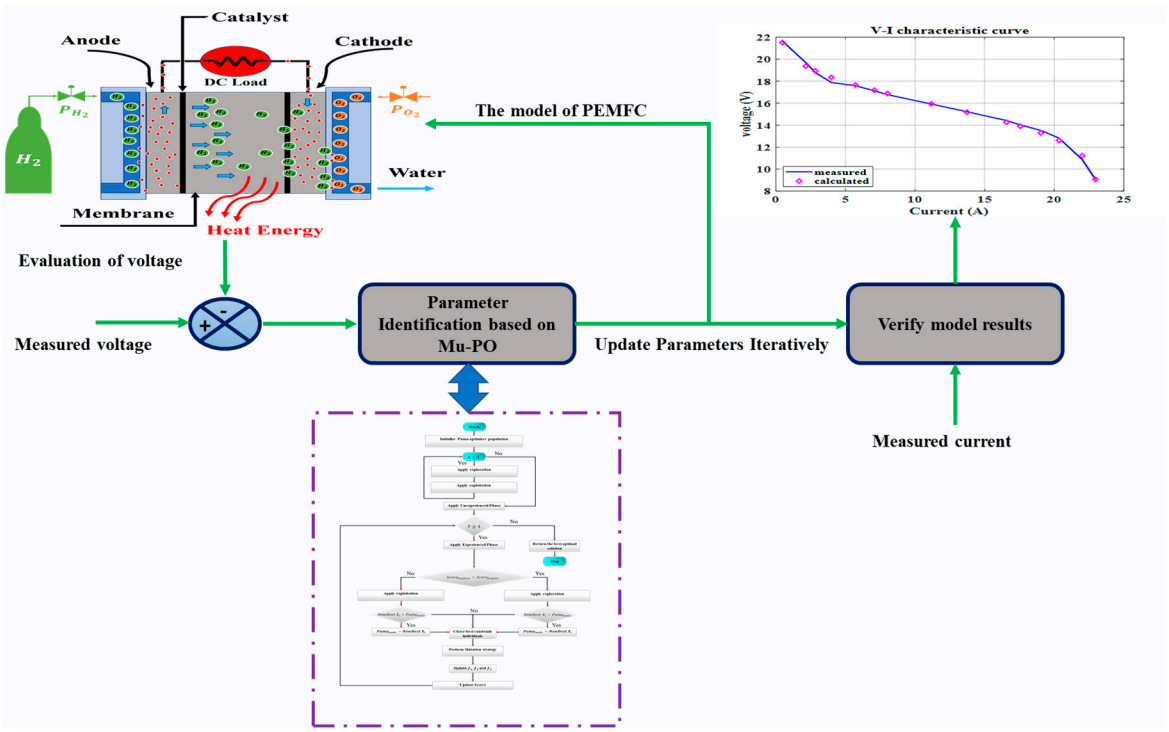

Figure 1. PEMFC parameter estimation procedure.

The problem of optimization is applied to the estimation of these parameters. This research aims to use the proposed Mu-PO approach to solve this optimization issue. The precision of the values of these acquired parameters must thus be expressed by the objective function (*Obj*) for this optimization.

The *Obj* in this study has been suggested as the sum of squared errors (SSE) between the measured and estimated voltages, and is represented in Equation (12) [20,36].

$$Obj = MinSSE(x) = Min\left(\sum_{i=1}^{k}[V_{st-mes} - V_{st-cal}]^2\right) \quad (12)$$

where k represents the number of data points, and V_{st-mes} and V_{st-cal} are the measured and calculated voltage of PEMFC.

3. Proposed Mutated Puma Optimization Algorithm

3.1. Mathematical Model of Puma Optimizer

The proposed puma optimizer algorithm simulates puma behavior. The acts made at every step are shown and modeled. This algorithm includes three stages, puma intelligence, exploration one, and exploration two.

3.1.1. Puma Intelligence

The suggested method's phase shift mechanism is a heuristic selection algorithm that performs award and punish scoring operations using two components: variety and intensification. The phase transition part was created by the cougars' intellect. It has two approaches:

- **Unexperienced phase**

Lacking sufficient energy and expertise, the cougars attempt to concurrently search for food by venturing into uncharted terrain. Until the phase change phase's setup is completed, the puma algorithm's exploration and exploitation operations are carried out concurrently during the first three iterations. In this part, just two functions ($f1$ and $f2$),

which are computed using Equations (13)–(16), have been used since the pair of exploitation and exploration phases are chosen in each iteration.

$$f1_{Explor} = PF_1 \cdot \left(\frac{Seq^1_{Cost\ Explore}}{Seq_{Time}} \right) \tag{13}$$

$$f1_{Exploit} = PF_1 \cdot \left(\frac{Seq^1_{Cost\ Exploit}}{Seq_{Time}} \right) \tag{14}$$

$$f2_{Explor} = PF_2 \cdot \left(\frac{Seq^1_{Cost\ Explore} + Seq^2_{Cost\ Explore} + Seq^3_{Cost\ Explore}}{Seq^1_{Time} + Seq^2_{Time} + Seq^3_{Time}} \right) \tag{15}$$

$$f2_{Exploit} = PF_2 \cdot \left(\frac{Seq^1_{Cost\ Exploit} + Seq^2_{Cost\ Exploit} + Seq^3_{Cost\ Exploit}}{Seq^1_{Time} + Seq^2_{Time} + Seq^3_{Time}} \right) \tag{16}$$

where Seq_{Time} is a variable with a constant value, PF_1 and PF_2 are fixed values, and $Seq^{1,2,3}_{Cost}$ values, which are connected to each of the phases of exploitation and exploration, are determined using Equations (17)–(22).

$$\mathrm{Seq}^1_{\mathrm{Cost\ Explore}} = \left| \mathrm{Cost}^{Initial}_{\mathrm{Best}} - \mathrm{Cost}^1_{\mathrm{Explore}} \right| \tag{17}$$

$$\mathrm{Seq}^2_{\mathrm{Cost\ Explore}} = \left| \mathrm{Cost}^2_{\mathrm{Explore}} - \mathrm{Cost}^1_{\mathrm{Explore}} \right| \tag{18}$$

$$\mathrm{Seq}^3_{\mathrm{Cost\ Explore}} = \left| \mathrm{Cost}^3_{\mathrm{Explore}} - \mathrm{Cost}^2_{\mathrm{Explore}} \right| \tag{19}$$

$$\mathrm{Seq}^1_{\mathrm{Cost\ Exploit}} = \left| \mathrm{Cost}^{Initial}_{\mathrm{Best}} - \mathrm{Cost}^1_{\mathrm{Exploit}} \right| \tag{20}$$

$$\mathrm{Seq}^2_{\mathrm{Cost\ Exploit}} = \left| \mathrm{Cost}^2_{\mathrm{Exploit}} - \mathrm{Cost}^1_{\mathrm{Exploit}} \right| \tag{21}$$

$$\mathrm{Seq}^3_{\mathrm{Cost\ Exploit}} = \left| \mathrm{Cost}^3_{\mathrm{Exploit}} - \mathrm{Cost}^2_{\mathrm{Exploit}} \right| \tag{22}$$

$\mathrm{Cost}^{Initial}_{\mathrm{Best}}$, the cost of the superior solution generated during the initialization step, together with six variables, is the best initial value. The costs of the best solution found during each of the stages of exploitation and exploration are repeated one, two, and three times, as follows: $\mathrm{Cost}^1_{\mathrm{Explore}}$, $\mathrm{Cost}^2_{\mathrm{Explore}}$, $\mathrm{Cost}^3_{\mathrm{Explore}}$, $\mathrm{Cost}^1_{\mathrm{Exploit}}$, $\mathrm{Cost}^2_{\mathrm{Exploit}}$, and $\mathrm{Cost}^3_{\mathrm{Exploit}}$.

From this point on, just one exploration and exploitation phase are chosen. Equations (23) and (24) are used to compute both locations of the exploitation and exploration phases so that pumas can select one of the two phases based on their positive experiences.

$$Score_{Explore} = \left(PF_1 \cdot f1_{Explor} \right) + \left(PF_2 \cdot f2_{Explor} \right) \tag{23}$$

$$Score_{Exploit} = \left(PF_1 \cdot f1_{Exploit} \right) + \left(PF_2 \cdot f2_{Exploit} \right) \tag{24}$$

- **Experienced phase**

Pumas finds that after three generations it is reasonable to decide to change phases. As they continue their iterations, they select only one phase for the optimization process. Three distinct functions—$f1$, $f2$, and $f3$—are utilized for scoring in this phase. Equations (25) and (26) is used to compute the first function.

$$f_1{}_t^{exploit} = PF_1 \cdot \left| \frac{Cost^{exploit}_{old} - Cost^{exploit}_{new}}{T^{exploit}_t} \right| \tag{25}$$

$$f_1{}_t^{explore} = PF_1 \cdot \left| \frac{Cost_{old}^{explore} - Cost_{new}^{explore}}{T_t^{explore}} \right| \quad (26)$$

The first function's quantity is dependent on the exploration or exploitation phase and is represented by $f_1{}_t^{exploit}$ and $f_1{}_t^{explore}$, whereas the costs of the optimal solution are represented by $Cost_{old}^{exploit}$ and $Cost_{old}^{explore}$.

Conversely, the expenses of the best option found after refining the current selection are represented by $Cost_{Old}^{exploit}$ and $Cost_{New}^{exploit}$. The numbers of not-chosen iterations from the prior selection to the present selection are $T_t^{explore}$ and $T_t^{exploit}$. Before the optimization procedure, the user-adjustable parameter PF_1 must be set with a value between 0 and 1.

The second function concentrates the resonance component, resulting in a phase that outperforms the other priority phase. Good performance is evaluated and assessed consecutively. As a result, this function may be useful throughout the exploitation phase of its selection. The second function is computed using (27) and (28):

$$f_2{}_t^{exploit} = PF_2 \cdot \left| \frac{\left(Cost_{Old,1}^{exploit} - Cost_{New,1}^{exploit}\right) + \left(Cost_{Old,2}^{exploit} - Cost_{New,2}^{exploit}\right) + \left(Cost_{Old,3}^{exploit} - Cost_{New,3}^{exploit}\right)}{T_{t,1}^{exploit} + T_{t,2}^{exploit} + T_{t,3}^{exploit}} \right| \quad (27)$$

$$f_2{}_t^{explore} = PF_2 \cdot \left| \frac{\left(Cost_{Old,1}^{explore} - Cost_{New,1}^{explore}\right) + \left(Cost_{Old,2}^{explore} - Cost_{New,2}^{explore}\right) + \left(Cost_{Old,3}^{explore} - Cost_{New,3}^{explore}\right)}{T_{t,1}^{explore} + T_{t,2}^{explore} + T_{t,3}^{explore}} \right| \quad (28)$$

where $Cost_{Old,1,2,3}^{explore}$ and $Cost_{Old,1.2.3}^{exploit}$ are the costs of the best option prior to improvement in the present choice for exploration and exploitation stages. $Cost_{New,1.2.3}^{explore}$ and $Cost_{New,1.2.3}^{exploit}$ represent the best option after the present choice exploration and exploitation stages. The numbers of unselected iterations from the prior choice to the present selection in each of the exploration and exploitation phases are denoted by $T_{t,1}^{explore}$ and $T_{t,2}^{exploit}$, where PF_2 is a fixed number with a value between 0 to 1.

Because choosing one phase results in collapsing into the local optimum trap, the third function of the choice mechanism highlights the diversity component and indicates that the phase that is not picked in many repetitions also has an opportunity to be selected. Equations (29) and (30) illustrate the function.

$$f_3{}_t^{exploit} = \begin{cases} if\ selected,\ f_3{}_t^{exploit} = 0 \\ otherwise,\ f_3{}_t^{exploit} + PF_3 \end{cases} \quad (29)$$

$$f_3{}_t^{explore} = \begin{cases} if\ selected,\ f_3{}_t^{explore} = 0 \\ otherwise,\ f_3{}_t^{explore} + PF_3 \end{cases} \quad (30)$$

Equation (15) states that if a stage is not chosen, the value of the third function in each of the exploitation and exploration phases will be raised by the parameter PF_3 in each iteration; if not, it will be set to zero. Before the optimization process, the user-adjustable PF_3 parameter has to be set to a value between 0 and 1.

The phase change function's cost is computed using Equations (31) and (32).

$$F_t^{exploit} = \left(\alpha_t^{exploit} \cdot \left(f_1{}_t^{exploit}\right)\right) + \left(\alpha_t^{exploit} \cdot \left(f_2{}_t^{exploit}\right)\right) + \left(\delta_t^{exploit} \cdot \left(\lfloor lc \rfloor \cdot f_3{}_t^{exploit}\right)\right) \quad (31)$$

$$F_t^{explore} = \left(\alpha_t^{explore} \cdot \left(f_1{}_t^{explore}\right)\right) + \left(\alpha_t^{explore} \cdot \left(f_2{}_t^{explore}\right)\right) + \left(\delta_t^{explore} \cdot \left(\lfloor lc \rfloor \cdot f_3{}_t^{explore}\right)\right) \quad (32)$$

lc, which covers a range of values other than zero numbers ($0 \notin lc$), is a collection of computed cost differences from the advances made throughout the exploration and

exploitation phases. During the search process, parameters α and δ for the exploration and exploitation phases are changeable based on the findings from each phase and are represented in Equations (33)–(36), respectively.

$$lc = \left\{ \{|Cost_{old} - Cost_{New}|\}^{exploitation} , \{|Cost_{old} - Cost_{New}|\}^{exploration} \right\}, 0 \notin lc \quad (33)$$

$$\alpha_t^{explore,\ exploit} = \begin{cases} if\ F^{exploit} > F^{explore},\ \alpha^{exploit} = 0.99,\ \alpha^{explore} = \left\lceil \alpha^{explore} - 0.01, 0.01 \right\rceil \\ otherwise,\ \alpha^{explore} = 0.99,\ \alpha^{exploit} = \left\lceil \alpha^{exploit} - 0.01, 0.01 \right\rceil \end{cases} \quad (34)$$

$$\delta_t^{exploit} = 1 - \alpha_t^{exploit} \quad (35)$$

$$\delta_t^{explore} = 1 - \alpha^{explore} \quad (36)$$

3.1.2. Exploration One

During exploration phase one, the puma algorithm uses the following equation to enhance its solutions after first sorting the total population in ascending order.

If $rand_1 > 0.5$, $Z_{i,G} = R_{Dim} * (Ub - Lb) + Lb$; otherwise

$$Z_{i,G} = X_{a,G} + G{\cdot}(X_{a,G} - X_{b,G}) + G{\cdot}(((X_{a,G} - X_{b,G}) - (X_{c,G} - X_{d,G})) + ((X_{c,G} - X_{d,G}) - (X_{e,G} - X_{f,G}))) \quad (37)$$

R_{Dim} represents randomly generated numbers that fall between 0 and 1 and correspond to the problem's dimensions.

Throughout the whole population, the solutions are represented by $X_{a,G}$, $X_{b,G}$, $X_{c,G}$, $X_{d,G}$, $X_{e,G}$, and $X_{f,G}$. Equation (38) is also used in the computation of G.

$$G = 2{\cdot}rand_2 - 1 \quad (38)$$

Next, the new solution is calculated using Equation (39).

$$X_{new} = \begin{cases} Z_{i,G}\ , \text{ if j} = \text{j}_{rand}\ or\ rand_3 \le U \\ X_{a,G},\ otherwise \end{cases} \quad (39)$$

where $Z_{i,G}$ denotes the solution chosen in Equation (37) and U is a parameter. Enhancing the solution is done by the requirement in Equation (40), which states that only the solutions' dimensions are updated if this condition is fulfilled.

$$if\ CostX_{new} < CostX_i,\ U = U + p \quad (40)$$

This action avoids the optimal location, and the outcome solutions are diverse, where p is represented in Equation (41).

$$p = \frac{NC}{Npop} \quad (41)$$

NC is a parameter calculated using Equation (41) and $Npop$ is population size.

$$NC = 1 - U \quad (42)$$

The crucial issue is that if the puma's output is not superior than the present pumas, Equation (39) will not be used since there is no reason to expand duplicate discoveries. However, high-quality solutions have seen few changes and aim to avoid falling into the trap of local optimality. Finally, the newly created solutions are substituted with the present solution using Equation (43).

$$X_{a,G} = X_{new},\ if\ X_{i,\ new} < X_{a,G} \quad (43)$$

3.1.3. Exploitation Two

The PO algorithm uses two separate operators to enhance the solutions, and these two methods are based on pumas' two hunt behaviors: ambush and dashing. Within nature, pumas attempt to ambush their prey among shrubs, trees, and rocks. In certain circumstances, the puma pursues its target, as reproduced by Equation (44).

$$X_{new} = \begin{cases} if\ rand_4 \geq 0.5,\ X_{new} = \frac{\left(\frac{mean(Sol_{total})}{Npop}\right)\cdot X_1^r - (-1)^{\beta} \times X_i}{1+(\alpha \cdot rand_5)} \\ otherwise, \\ if\ rand_6 \geq L,\ X_{new} = Puma_{male} + (2 \cdot rand_7) \cdot exp(randn_1) \cdot X_2^r - X_i \\ otherwise, \\ X_{new} = (2 \times rand_8) \times \frac{(F_1 \cdot R \cdot X(i) + F2 \cdot (1-R) \cdot Puma_{male})}{(2 \cdot rand_9 - 1 + randn_2)} - Puma_{male} \end{cases} \quad (44)$$

Sol_{total} is the total value of all solutions. X_1^r is a randomly picked solution from the whole population, and β is a zero or one generated at random. Furthermore, X_i represents the current solution in the current iteration, whereas α and L are static parameters. Furthermore, $Puma_{male}$ is the most effective solution for the whole population.

In the end, Equations (45)–(47) compute R, F1, and F2.

$$R = 2 \cdot rand_{11} - 1 \quad (45)$$

$$F_1 = randn_3 \cdot exp\left(2 - Iter \cdot \left(\frac{2}{MaxIter}\right)\right) \quad (46)$$

$$F_2 = w \times (v)^2 \cdot cos((2 \times rand_{12}) \cdot w) \quad (47)$$

where w and v, are random values between 0 and 1, and $MaxIter$ represents the maximum iterations; see [31].

Figure 2 displays the traditional flowchart for PO approach. For further details on the proposed Mu-PO algorithm, the flow chart is presented in Figure 3.

3.1.4. Mutation Strategy

Differential evolution (DE) operates in two stages: initiation and evolution. Initially, the population is formed randomly; then, in the evolution phase, the population undergoes mutation, crossover, and selection processes, which are iterated until the termination requirements are satisfied [37].

One of the most crucial stages we need in the hybridization process is the mutation operation established in this study.

Following exploitation and exploration, a mutation is performed to create a new vector called the mutation vector.

In mutation, a mutant vector V_i is generated for each target vector x_i, and it is chosen from the current population as the best cost vector as follows:

$$V_i = x_{r1}^*(t) + F \cdot (x_{r2}^*(t) + x_{r3}^*(t)) \quad (48)$$

where F represents the scaling factor and its value varies from 0 to 1, where $r1$, $r2$, and $r3$ are distinct random values selected from the set {1, 2,..., $Npop$}, ensuring they are also different from the current value.

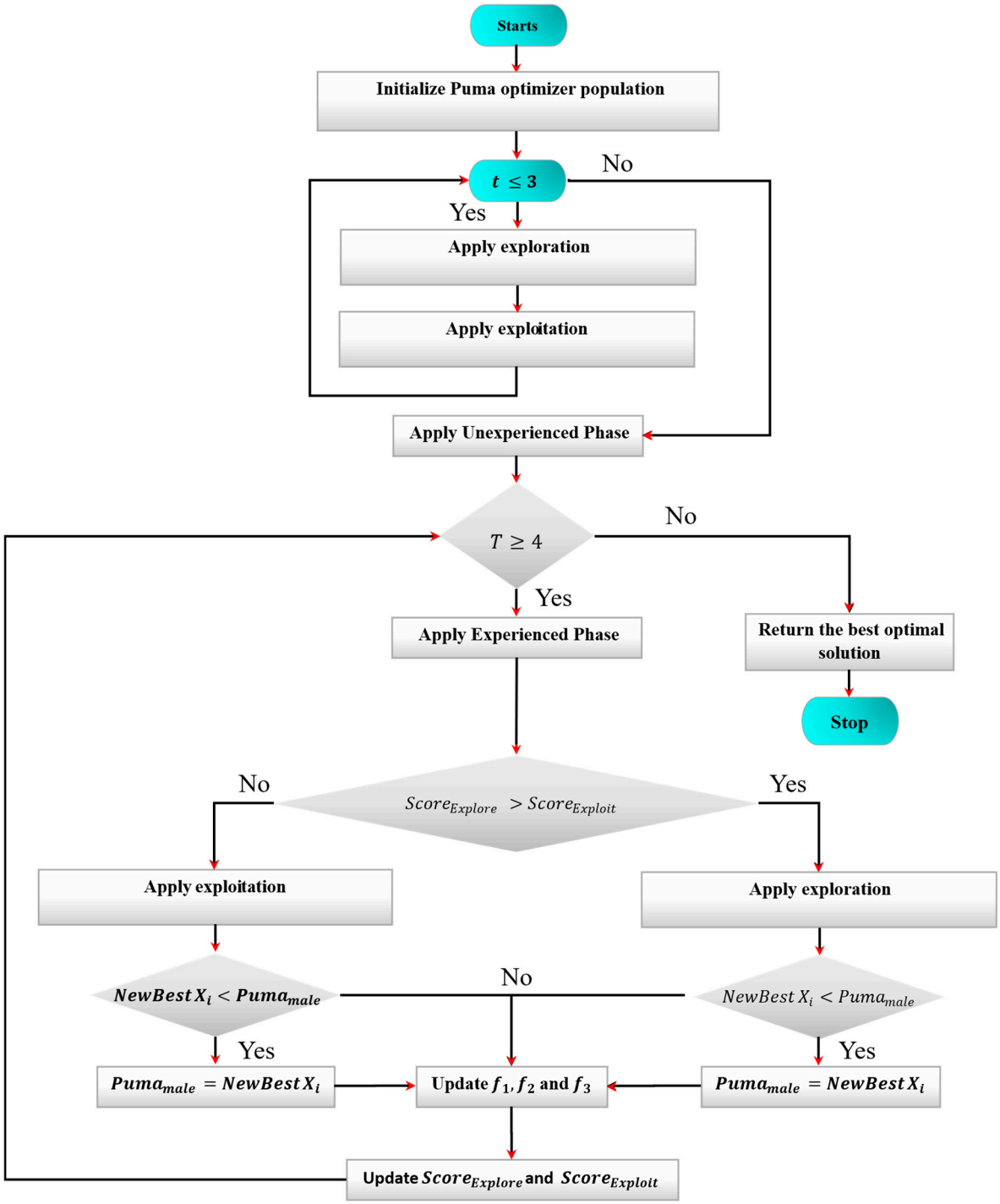

Figure 2. Conventional puma optimizer flowchart.

The purpose of integrating the mutation stage is to enhance population diversity and introduce controlled perturbations, thereby improving the global exploration capability of the algorithm. Specifically, after the extraction phase of the original PO, the mutation operator generates a modified candidate vector, which is then evaluated using the same cost function defined in Equation (48). If the mutated solution yields a better fitness value than the corresponding individual in the PO population, it replaces the original; otherwise, the original PO solution is retained for the next generation. This mechanism enables the algorithm to escape local minima and maintain a better balance between exploration and exploitation, reducing the risk of premature convergence in complex multimodal search spaces.

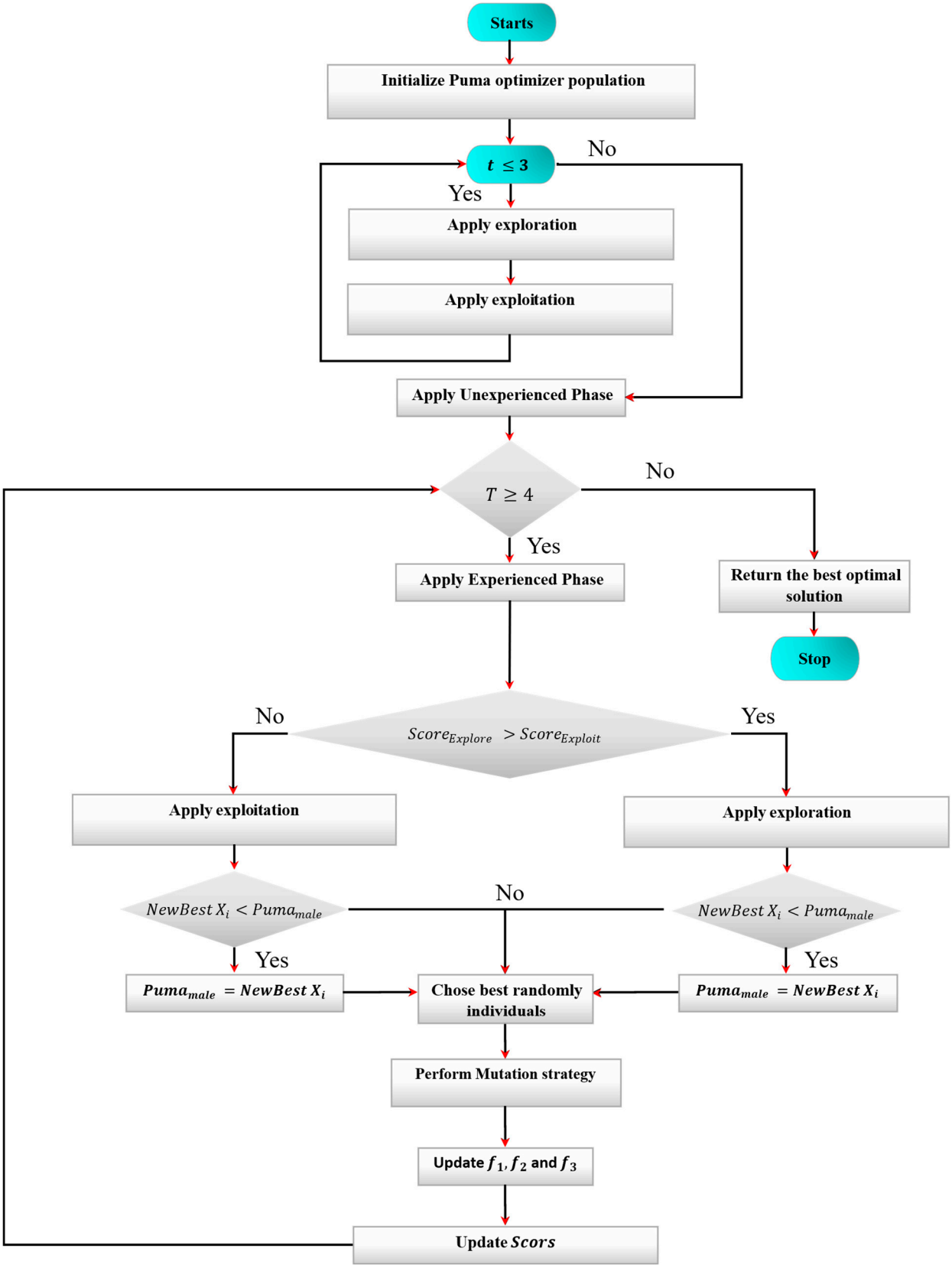

Figure 3. The proposed mutated puma optimizer flowchart.

4. Results and Discussion

Using three distinct commercial and experimental datasets for PEMFCs—250 W, SR-12, and NedStack PS6 [38,39]—with distinct features and research boundaries listed in Table 1, we validated the suggested algorithm PO. The population size and maximum number of iterations were set to 30 and 500. The Mu-PO algorithm's convergence is compared to other standard meta-heuristic algorithms, such as BO, DE, FFA, and BBO. Table 2 describes the algorithmic parameters for these methods. It is commonly known that meta-heuristics are very random. Consequently, the exhibited minimal SSE results are obtained across 30 separate executions, in addition to performance measurements to ensure the accuracy as described by the metrics as follows: standard deviation (*SD*), mean absolute error (*MAE*), relative error (*RE*), and root mean square error (*RMSE*). These measures are represented in Equations (49)–(52), with n set to 30, related to the number of independent runs [40].

$$SD = \sqrt{\frac{\sum_{j=1}^{30}\left(SSE_J - SSE_{men}\right)}{30-1}} \tag{49}$$

$$MAE = \frac{\sum_{j=1}^{30}\left(SSE_j - SSE_{min}\right)}{30} \tag{50}$$

$$RE = \frac{\sum_{j=1}^{30}\left(SSE_j - SSE_{min}\right)}{SSE_{min}} \tag{51}$$

$$RMSE = \sqrt{\frac{\sum_{j=1}^{30}\left(SSE_J - SSE_{min}\right)^2}{30}} \tag{52}$$

Table 1. Features of commercial PEMFC stacks and the seven parameters' boundaries.

Search Limits			PEMFC Parameters	250 W	SR-12	NedStack PS6
Parameters	**Lower value**	**Upper value**	N	24	48	65
δ_1	−1.1997	−0.8532	A	27	62.5	240
δ_2	0.001	0.005	L	127	0.25	178
δ_3 (10^{-5})	3.9	9.8	T_{fc}	343.15	323	343
δ_4 (10^{-4})	−2.6	−9.54	P_{O2}	1	0.2095	1
λ	10	23	P_{H2}	1	1.47628	1
R_c (mΩ)	0.1	0.8				
β (10^{-2})	1.36	50				

Table 2. Algorithms' parameters.

Algorithm	Parameter	Value
BO	Sharing coefficient for alpha bonobo. Sharing coefficient for selected bonobo Value of temporary sub-group size factor. Initial probability for extra-group mating	$Scab$ = 1.25 $Scsb$ = 1 $tsgs_{factor\_max}$ = 0.05 $p_{xgm\_initial}$ = 0.03
DE	Crossover probability	P_{cr} = 0.6
FFA	Number of sections	K = 2
BBO	Keep rate	Kr = 0.2
PO and Mu-PO	PF_1 PF_2 PF_3	0.5 0.5 0.3

4.1. Convergence Curves and Statistical Measurements

Figure 4 shows the convergence curves for the optimal SSE values for PEMFC stacks using the hybrid Mu-PO algorithm in comparison with traditional PO, BO, DE, FFA, and BBO. Mu-PO has a fast convergence as shown in Figure 4a for a 250 W PEFMC, while in Figure 4b, concerning SR-12, the proposed algorithm reaches its SSE in approximately 10 iterations as presented, and the same result was obtained for the NedStack PS6 PEMFC model. It is observed that the suggested method attained a local minima before reaching the global lowest value of the goal function. Based on the statistical measures presented in this part, it is possible to determine that the proposed algorithm was successful in demonstrating its resilience in addressing the optimization issue of identifying PEMFC parameters. The Mu-PO approach outperformed existing algorithms in the literature, including traditional PO, BO, DE, FFA, and BBO. Table 3 shows several metrics (minimum, average, maximum, SD, MAE, RE, and RMSE) for different techniques. Based on these findings, it is clear that Mu-PO was successful in achieving the best minimal SSE value for all of the examined PEMFC stacks. To prove the robustness of Mu-PO, the SD measured of Mu-PO for all PEMFCs tested is equal to 8.618089×10^{-14}, 6.144751×10^{-8}, and 7.315949×10^{-14}, which is significantly lower than the values of the traditional PO, which confirms the robustness of the proposed algorithm throughout 30 independent runs.

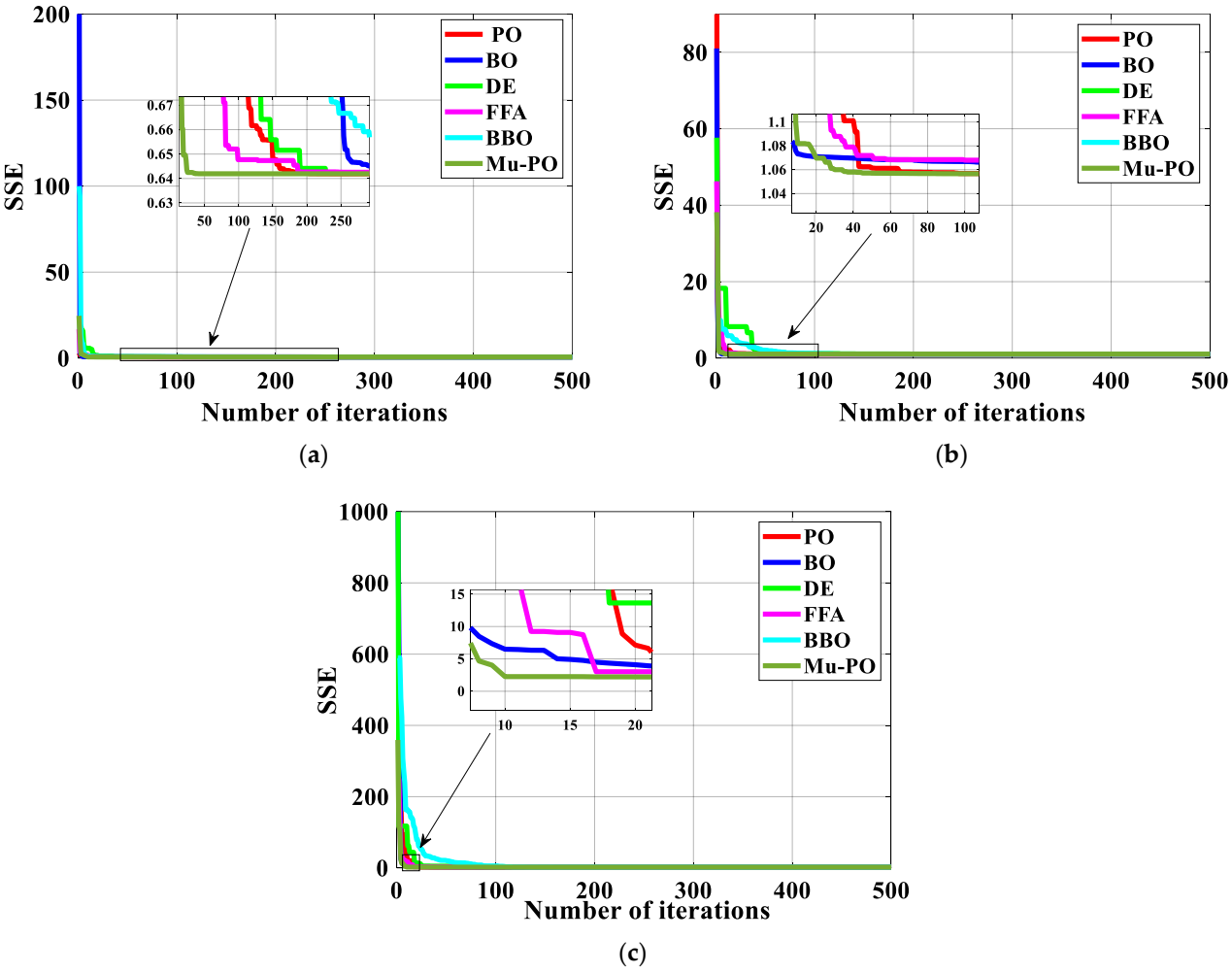

Figure 4. Convergence curves for SSE_{min}: (**a**) 250 W, (**b**) SR-12, (**c**) NedStack PS6.

Table 3. Statistical measures of the suggested Mu-PO for different PEMFCs were compared to various meta-heuristic algorithms.

PEMFC Model	Algorithms	Best SSE	Mean SSE	Worst SEE	SD	MAE	RE	RMSE
250 W	**Mu-PO**	**0.641930**	**0.641930**	**0.641930**	$\mathbf{8.618089 \times 10^{-14}}$	$\mathbf{2.401782 \times 10^{-14}}$	$\mathbf{1.122449 \times 10^{-12}}$	$\mathbf{8.807057 \times 10^{-14}}$
	PO	0.641930	0.641930	0.641930	3.719319×10^{-10}	9.529510×10^{-11}	4.453553×10^{-9}	3.778987×10^{-10}
	BO	0.641970	0.649967	0.863434	4.040662×10^{-2}	0.0079965	0.373687	4.052427×10^{-2}
	DE	0.641936	0.641964	0.642044	2.797120×10^{-5}	0.6301080	29.447232	3.946281×10^{-5}
	FFA	0.642103	0.647558	0.680695	9.678950×10^{-3}	5.455590×10^{-3}	0.254893	1.096917×10^{-2}
	BBO	0.642117	0.646627	0.676569	8.296032×10^{-3}	4.510089×10^{-3}	0.210713	9.320457×10^{-3}
	PKO [41]	0.6419309	0.6419309	0.6419309	2.31727×10^{-8}	6.03551×10^{-9}	2.82063×10^{-7}	2.35691×10^{-8}
	MAEO [42]	0.642024	0.642868	0.652231	0.209969	0.000844028	3.943907×10^{-2}	2.230283×10^{-3}
	ISAA [40]	0.6434	0.869800	1.8744	19.96834	0.226405	35.18761	0.301221
	TGA [19]	0.749606	1.893472	1.22002412	29.777932	0.470417	18.82655	0.554084
	MMEFO [38]	0.6420829	0.658273	0.757570877	2.582516	1.619012×10^{-2}	0.756450	0.030113
SR-12	**Mu-PO**	**1.056628**	**1.056628**	**1.056628**	$\mathbf{6.144751 \times 10^{-8}}$	$\mathbf{1.129559 \times 10^{-8}}$	$\mathbf{3.207067 \times 10^{-7}}$	$\mathbf{6.146159 \times 10^{-8}}$
	PO	1.056628	1.057688	1.081319	4.614328×10^{-3}	1.060309×10^{-3}	3.010450×10^{-2}	4.659028×10^{-3}
	BO	1.056736	1.067304	1.116991	1.441994×10^{-2}	1.056718×10^{-2}	0.2999946	1.768244×10^{-2}
	DE	1.057928	1.058305	1.062971	1.457654×10^{-3}	1.067230×10^{-2}	3.763512×10^{-4}	1.481746×10^{-3}
	FFA	1.061778	1.067209	1.118766	1.355050×10^{-2}	5.430931×10^{-3}	0.1534481	1.438717×10^{-2}
	BBO	1.059169	1.062814	1.072437	4.484731×10^{-3}	3.644481×10^{-3}	0.1032265	5.720544×10^{-3}
	MAEO [42]	1.056633	1.061733	1.074281	0.434743	5.100260×10^{-3}	0.1448069	6.654537×10^{-3}
	P-DSO [20]	1.0639	NA	NA	NA	NA	NA	0.243
	TGA [19]	1.104085	2.063522	5.504109	99.239232	0.959437	26.069652	1.368405
	CHHO4 [43]	1.057160	5.230704	32.606272	826.24227	4.173544	197.39415	9.182633
NedStack PS6	**Mu-PO**	**2.079165**	**2.079165**	**2.079165**	$\mathbf{7.315949 \times 10^{-14}}$	$\mathbf{4.041211 \times 10^{-14}}$	$\mathbf{5.831009 \times 10^{-13}}$	$\mathbf{8.250360 \times 10^{-14}}$
	PO	2.079165	2.083101	2.175294	1.786653×10^{-2}	3.935483×10^{-3}	5.678456×10^{-2}	1.800168×10^{-2}
	BO	2.079361	2.225639	3.968874	0.3768642	0.146277	2.110416	0.398358
	DE	2.096216	2.153803	2.205221	3.6063670×10^{-2}	5.758728×10^{-2}	0.824160	6.762788×10^{-2}
	FFA	2.188748	2.202313	2.428657	6.1687763×10^{-2}	1.356482×10^{-2}	0.185925	6.214932×10^{-2}
	BBO	2.1936108	2.206590	2.206590	7.1519440×10^{-2}	1.297935×10^{-2}	0.177506	7.150519×10^{-2}
	MVO [26]	2.3632	3.7385	4.3803	0.8221	NA	NA	NA
	RTH [44]	2.1058	2.1058	2.1058	1.79×10^{-6}	NA	NA	NA
	P-DSO [20]	2.1457	NA	NA	NA	NA	NA	0.123
	STSA [45]	2.14576	2.35539	3.18282	0.27994	0.20895	NA	NA

Note: Values in bold correspond to results obtained using the proposed Mu-PO algorithm for each PEMFC model.

Figure 5 shows the SSE results from 30 separate runs for the proposed Mu-PO and the traditional PO for the three commercial PEMFC stacks (250 W, SR-12 and NedStack PS6), demonstrating the consistency and dependability of the proposed Mu-PO.

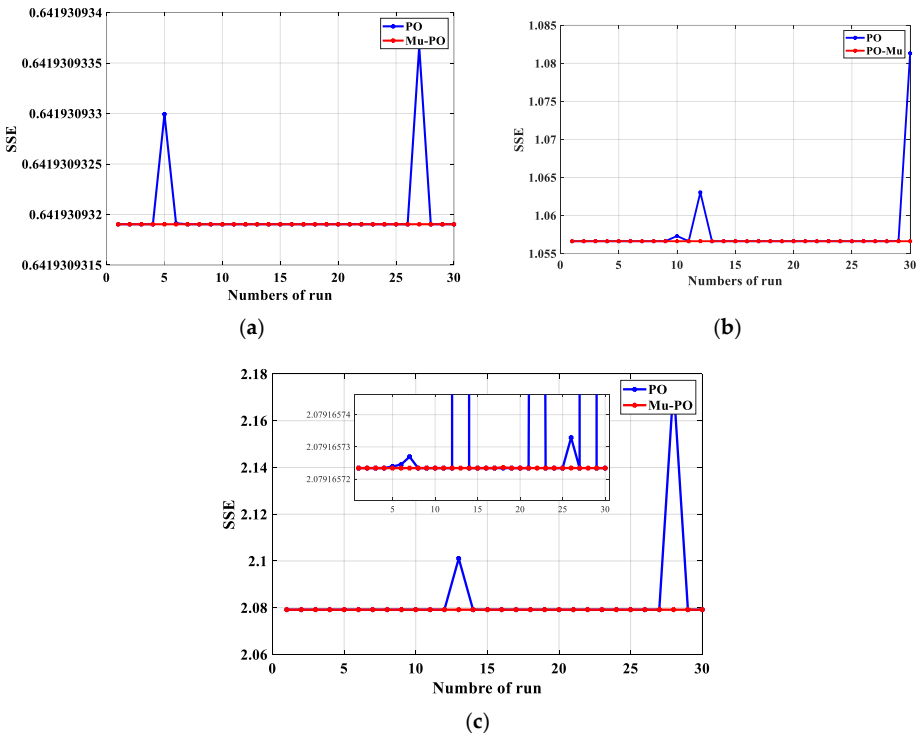

Figure 5. Multiple independent runs of SSE for (**a**) 250 W, (**b**) SR-12, (**c**) NedStack PS6.

4.2. Parameter Identification for Commercial PEMFC Types

The P-I and V-I-polarization curves for the three types of PEMFC are displayed in Figure 6. To confirm the effectiveness of the adjusted settings, these polarization graphs have been compared to those from each of the three PEMFC stacks. All curves confirmed the coincidence of the calculated curves over the experimental curves, demonstrating the proposed Mu-PO accuracy in handling the optimization issue of identifying seven unknown parameters of different PEMFCs. The model's polarization curves closely matched those obtained from experimental data, demonstrating the correctness of the suggested Mu-PO-based PEMFC model.

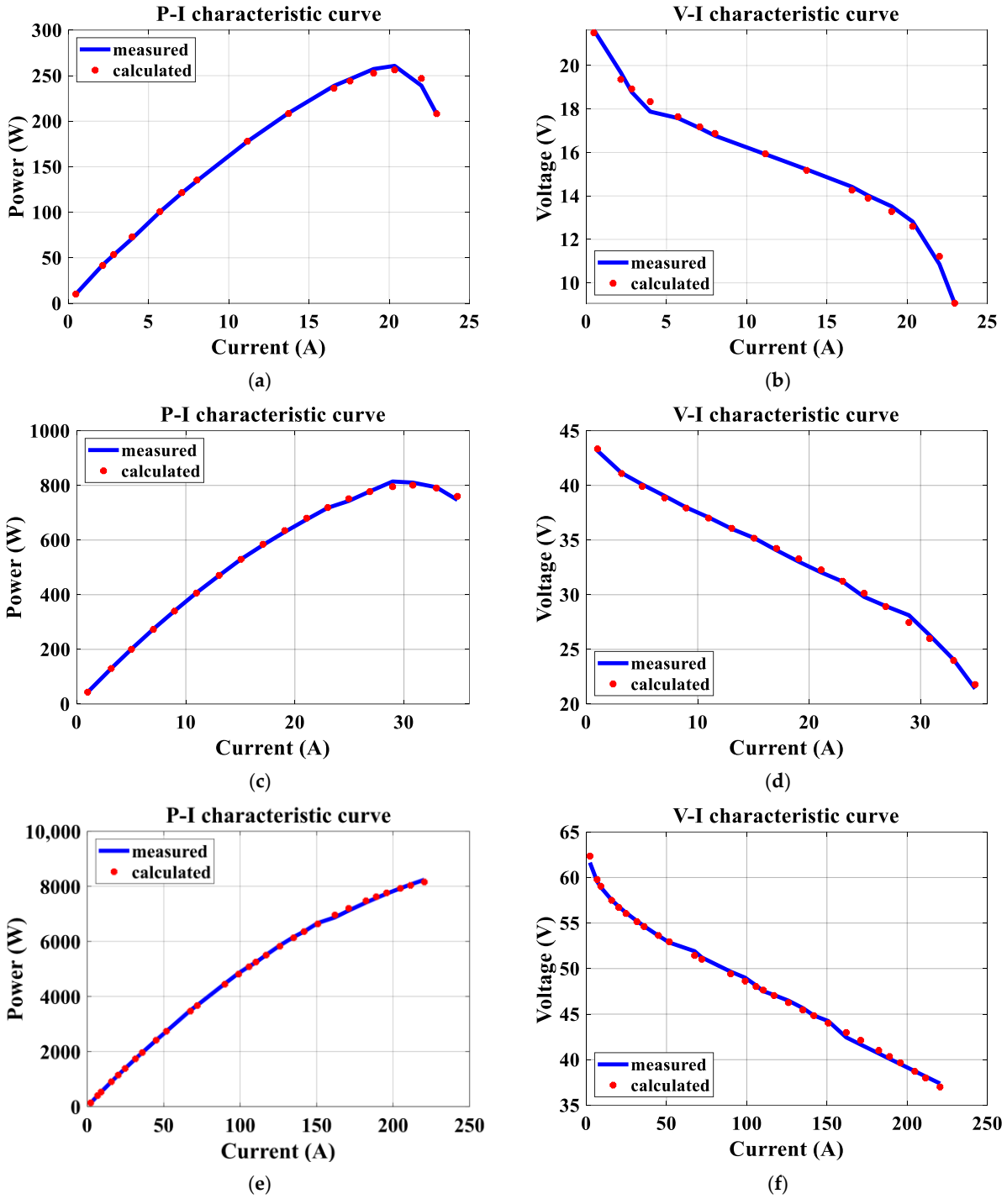

Figure 6. Characteristic curves: (**a**,**b**) P-I and V-I curves for 250 W, (**c**,**d**) P-I and V-I curves for SR-12, (**e**,**f**) V-I and V-I curves for NedStack PS6.

Table 4 shows the optimized seven parameter values for the 250 W PEMFC, SR-12, and NedStack PS6 using the suggested Mu-PO and other present-day optimization techniques. In the scenario of a 250 W PEMFC, the suggested algorithm produces an SSE of 0.641930, proving the suitability of the proposed algorithm regarding other optimization methods such as BO, which gives 0.641970; DE, which gives a minimum SSE of 0.641936; FFA, which generates a minimum SSE of 0.642103; and BBO, which gives the value of 0.642117. In contrast to existing optimization algorithms in the literature, the suggested algorithm performs better in addressing the optimization issue, resulting in the best value of the objective function. For the second PEMFC type, SR-12 500 W, the suggested Mu-PO contributes to achieving the global minimum of the objective function of 1.056628, demonstrating the superior overall optimization procedures stated in Table 4. Likewise, in the final scenario of NedStack PS6, the suggested algorithm produces the lowest value of SSE, equal to 2.079165, putting it in competition with BO, DE, FFA, BBO, and another optimization techniques in the literature.

Table 4. Mu-PO optimization results for several PEMFCs are compared to other recently developed optimization techniques.

PEMFC Model	Algorithms	δ_1	$\delta_2 \times 10^{-3}$	$\delta_3 \times 10^{-5}$	$\delta_4 \times 10^{-4}$	λ	β	$R_m \times 10^{-3}$	Best SSE
250 W	**Mu-PO**	**−0.87687351**	**2.39397288**	**5.7723139394**	**−1.558841**	**23.000000**	**0.0545547**	**0.100000**	**0.641930**
	PO	−1.181642	3.006078	3.799094	−1.558841	22.999999	0.054554	0.100000	0.641930
	BO	−1.080811	3.064543	6.319581	−1.556242	22.999999	0.054607	0.100000	0.641970
	DE	−1.0563241	2.951741	6.020298	−1.559301	23.000000	0.054562	0.100000	0.641936
	FFA	−1.159784	3.663832	8.949574	−1.562713	22.999974	0.054534	0.100020	0.642103
	BBO	−1.047146	2.957754	6.259910	−1.554231	23.000000	0.054599	0.100000	0.642117
	PKO [41]	−0.8559524	2.0292167	3.6007777	−1.5588414	22.99999	0.054554	0.0545547	0.641930
	MAEO [42]	−0.89119	2.264152	3.84106	−1.55950	22.999999	0.05454	0.100019	0.64202
	ISAA [40]	−0.8616	3.1548	9.7857	−1.5423	22.8812	0.0547	0.10016	0.6434
	TGA [19]	−1.1914	4.1129	6.0573	−1.7090	18.689	0.0544	0.48527	0.7496
	MMEFO [38]	−1.06414	3.244598	6.73197	−1.56013	18.36909	0.05452	0.226552	0.64208
SR-12	**Mu-PO**	**−1.18016500**	**3.806371**	**6.877702**	**−0.954000**	**23.000000**	**0.175320**	**0.672627**	**1.056628**
	PO	−0.883910	3.321399	9.673095	−0.954000	23.000000	0.175320	0.672627	1.056628
	BO	−1.133570	4.110560	9.779971	−0.954000	23.000000	0.175751	0.651024	1.056736
	DE	−1.110843	3.332806	5.198301	−0.954000	23.000000	0.174275	0.743480	1.057928
	FFA	−1.042288	3.598483	8.300784	−0.959947	19.376851	0.177436	0.49100	1.061778
	BBO	−1.189542	4.164633	9.002208	−0.954000	19.335350	0.173564	0.695557	1.059169
	MAEO [42]	−0.86068	2.77134	6.19649	−0.954009	22.98870	0.175366	0.670732	1.056633
	P-DSO [20]	−1.1982	3.3570	3.6000	−0.9.5416	20.2746	0.1719	0.8.0000	1.0639
	TGA [19]	−1.112395	3.854663	4.369857	−0.964482	23	0.18307	0.218868	1.104085
	CHHO4 [43]	−0.85320	3.091841	8.238772	−0.9540	22.911559	0.176237	0.624684	1.057160
NedStack PS6	**Mu-PO**	**−0.8762888**	**3.333139**	**9.7998406**	**−0.9540000**	**13.094707**	**0.0136000**	**0.10000**	**2.0791657**
	PO	−0.901855	2.540385	3.600000	−0.954000	13.094707	0.013600	0.100000	2.079165
	BO	−1.092124	3.521869	6.649671	−0.954000	13.088485	0.013600	0.100000	2.0793619
	DE	−0.979150	3.081539	5.862539	−0.954000	13.358934	0.0185124	0.100000	2.0962163
	FFA	−0.944612	2.774281	4.381349	−0.954062	18.777589	0.084945	0.101377	2.1887488
	BBO	−1.107961	3.808536	8.373130	−0.954000	20.447652	0.097349	0.100000	2.1936108
	MVO [26]	−1.0394	3.2439	5.77	−0.9540000	16.1317	0.0290	0.171	2.3632
	RTH [44]	−0.90568	3.44	8.76	−0.900000	17.80574	0.08185	0.8	2.1058
	P-DSO [20]	−1.0062	3.0823	5.3097	−0.95400	19.7906	0.0136	0.10000	2.1457
	STSA [45]	−0.8532	2.84	6.79	−0.954	13.46327	0.0136	0.100	2.14576

Note: Values in bold correspond to results obtained using the proposed Mu-PO algorithm for each PEMFC model.

4.3. The Dynamic Behavior of PEMFCs

Temperature fluctuations significantly impact the stability of identified parameters, particularly on charge transfer coefficients (δ_1, δ_2) and membrane resistance (R_m), as evidenced by the adaptive temperature–PEMFC durability model. This section examines the impact of varying PEMFC stack temperature and reactant pressure to validate the optimized parameters and assess how modifying these factors influences the PEMFC stack's

operating characteristic curves. The comparison of numerical results and experimental data for the PEMFC under different degradation levels is performed in ref. [46], while in reference [47] the authors focus on quantifying the parameter reliability. The performance of the 250 W PEMFC, SR-12 PEMFC, and NedStack PS6 is evaluated under different cell temperatures and reactant pressures. First, the temperature impact is evaluated at different temperatures, while reactant pressures are set to the levels shown in Table 1. Temperature-dependent polarization curves are shown in Figure 7. Furthermore, the influence of the reactants' pressure on the polarization curves of the PEMFCs has been investigated by applying various pressure values while maintaining the stack's temperature fixed at the values indicated in Table 1. Figure 8 depicts pressure-dependent polarization curves. Figure 7a–c show that raising the operating temperature at constant supply pressures improves the polarization characteristics. Similarly, Figure 8a–c illustrate that increasing the input pressures at a fixed cell temperature improves the output voltage.

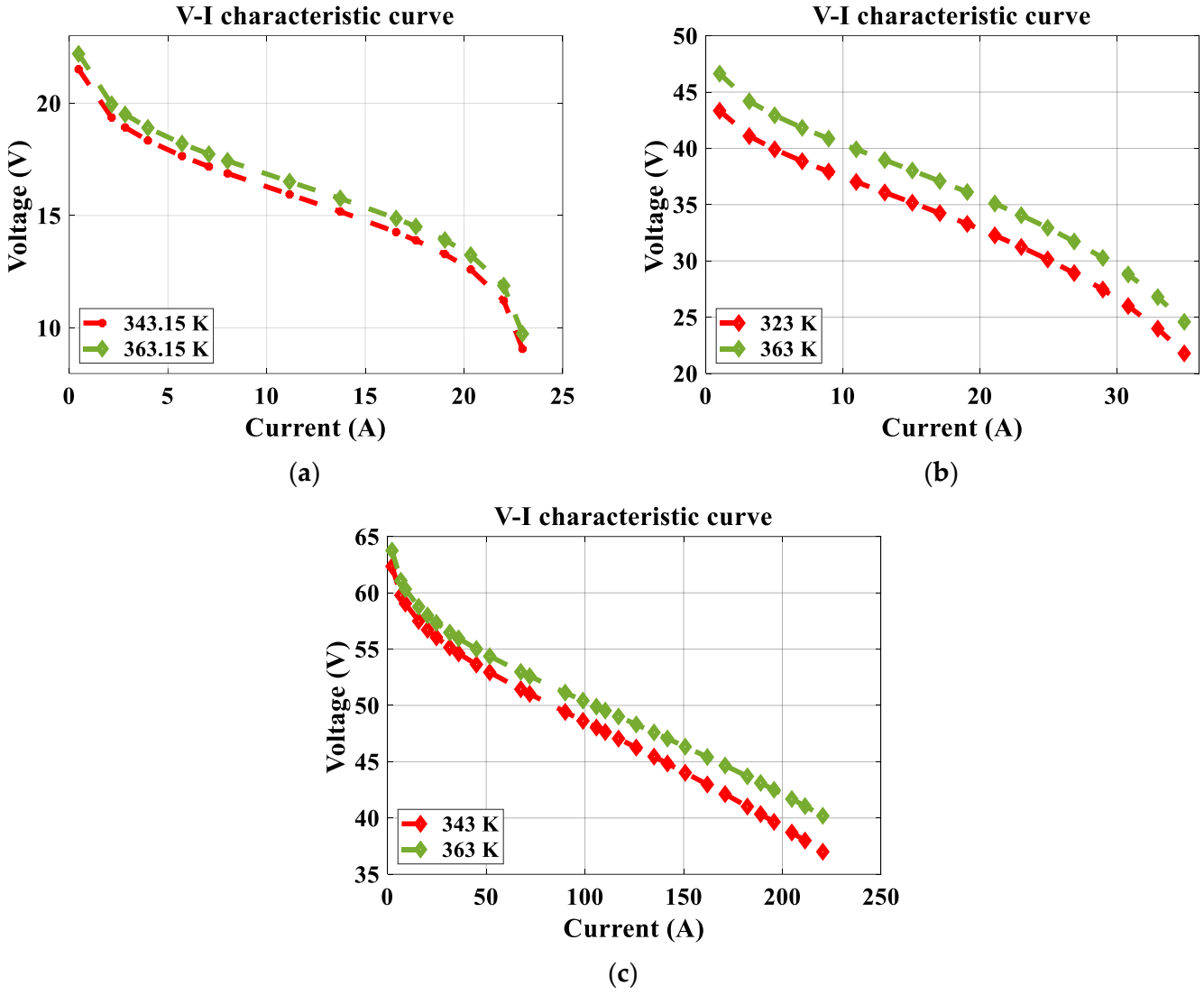

Figure 7. Dynamic functioning of different PEMFCs at varied temperature values: (**a**) V-I curve for 250 W, (**b**) V-I curve for SR-12, (**c**) V-I curve for NedStack PS6.

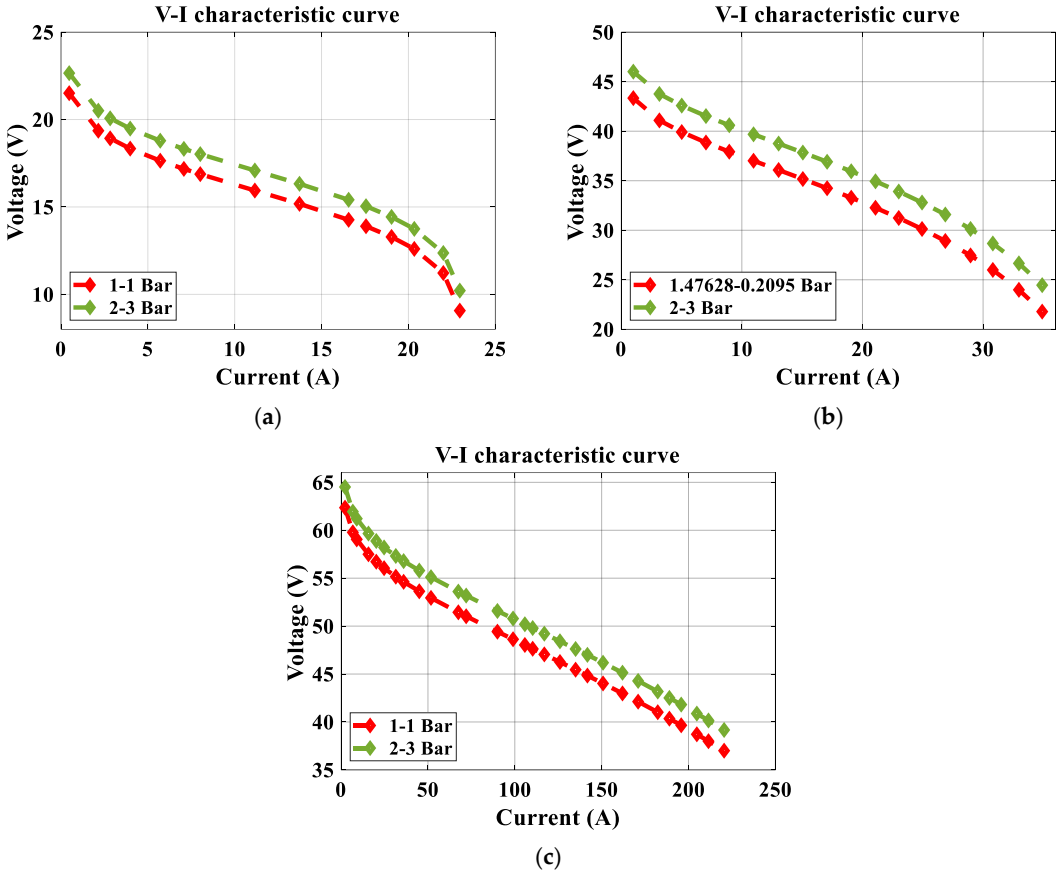

Figure 8. Dynamic functioning of different PEMFCs at varied pressure values: (**a**) V-I curve for 250 W, (**b**) V-I curve for SR-12, (**c**) V-I curve for NedStack PS6.

5. Conclusions

An effective optimized approach known as Mu-PO has been proposed for extracting the seven unknown parameters of the well-established Amphlett PEMFC model. The proposed method was validated using three commercial PEMFC stacks: 250 W PEMFC, SR-12 500 W PEMFC, and NedStack PS6. The strong agreement between the model-predicted and experimentally measured polarization curves demonstrates the effectiveness of the Mu-PO algorithm in minimizing the sum of squared errors (SSE). The proposed algorithm consistently achieved lower SSE values compared to widely adopted algorithms, including BO, DE, FFA, and BBO. Specifically, the SSE values obtained for the 250 W, SR-12 500 W, and NedStack PS6 stacks were 0.641930, 1.056628, and 2.079165, respectively in less iterations in comparison with traditional PO, highlighting the superior accuracy of the proposed approach. In addition to achieving optimal parameter estimates, the MU-PO algorithm exhibited significant improvements in convergence speed and solution stability in comparison with traditional PO. Statistical analysis further validated Mu-PO's consistency and resilience across multiple optimizations runs, outperforming other contemporary algorithms in terms of both accuracy and robustness. The results confirm that the algorithm is capable of handling nonlinear optimization. Given its demonstrated performance, the Mu-PO algorithm presents a promising tool for addressing complex optimization challenges, including parameter identification in PEMFC models. The efficacy of Mu-PO in actual applications generally depends on the type of PEMFC stack and environmental conditions that may adversely affect the algorithm. Furthermore, further investigation is necessary to evaluate the scalability of Mu-PO to larger PEMFC stacks or more complex, high-dimensional optimization problems. Moreover, future studies

will focus on advancing the proposed parameter identification approach for practical implementation in PEM fuel cell (PEMFC) systems. The identified parameters can be applied to real-time control, enabling adaptive and resilient strategies capable of responding to variations in operating conditions and system aging. The method can also support lifetime prediction and state-of-health assessment, by monitoring parameter changes as indicators of degradation processes. Furthermore, the approach may be integrated into fault diagnosis and fault-tolerant control frameworks, allowing early detection of abnormal behaviors and enhancing system reliability. These developments aim to bridge offline parameter identification with the real-world operation of PEMFC systems, highlighting the practical relevance and applicability of the proposed approach.

Author Contributions: Conceptualization, N.R., B.K., A.L., S.N., S.A.D. and K.Y.; Methodology, N.R., A.L., S.A.D. and K.Y.; Software, N.R., B.K., A.L., S.A.D. and K.Y.; Validation, N.R., B.K., S.N., S.A.D. and K.Y.; Formal analysis, N.R. and S.N.; Investigation, N.R., B.K., S.N. and S.A.D.; Resources, N.R., A.L. and S.A.D.; Data curation, N.R., B.K., A.L. and S.N.; Writing—original draft, N.R., S.A.D. and K.Y.; Writing—review & editing, B.K., A.L. and S.N.; Supervision, K.Y. All authors have read and agreed to the published version of the manuscript.

Funding: This research received no external funding.

Data Availability Statement: The original contributions presented in this study are included in the article. Further inquiries can be directed to the corresponding author.

Conflicts of Interest: The authors declare no conflict of interest.

References

1. Sharaf, O.Z.; Orhan, M.F. An Overview of Fuel Cell Technology: Fundamentals and Applications. *Renew. Sustain. Energy Rev.* **2014**, *32*, 810–853. [CrossRef]
2. Saebea, D.; Chaiburi, C.; Authayanun, S. Model Based Evaluation of Alkaline Anion Exchange Membrane Fuel Cells with Water Management. *Chem. Eng. J.* **2019**, *374*, 721–729. [CrossRef]
3. Oryshchyn, D.; Harun, N.F.; Tucker, D.; Bryden, K.M.; Shadle, L. Fuel Utilization Effects on System Efficiency in Solid Oxide Fuel Cell Gas Turbine Hybrid Systems. *Appl. Energy* **2018**, *228*, 1953–1965. [CrossRef]
4. İnci, M.; Türksoy, Ö. Review of Fuel Cells to Grid Interface: Configurations, Technical Challenges and Trends. *J. Clean. Prod.* **2019**, *213*, 1353–1370. [CrossRef]
5. Yang, B.; Wang, J.; Yu, L.; Shu, H.; Yu, T.; Zhang, X.; Yao, W.; Sun, L. A Critical Survey on Proton Exchange Membrane Fuel Cell Parameter Estimation Using Meta-Heuristic Algorithms. *J. Clean. Prod.* **2020**, *265*, 121660. [CrossRef]
6. Fathy, A.; Rezk, H.; Alharbi, A.G.; Yousri, D. Proton Exchange Membrane Fuel Cell Model Parameters Identification Using Chaotically Based-Bonobo Optimizer. *Energy* **2023**, *268*, 126705. [CrossRef]
7. Priya, K.; Sathishkumar, K.; Rajasekar, N. A Comprehensive Review on Parameter Estimation Techniques for Proton Exchange Membrane Fuel Cell Modelling. *Renew. Sustain. Energy Rev.* **2018**, *93*, 121–144. [CrossRef]
8. Han, C.; Hu, L.; Ouyang, D.; Wang, Z. Research on Thermal Runaway Warning Threshold and Machine Learning Model for Large Capacity Energy Storage Batteries Based on Electric-Thermal-Mechanical-Gas Coupling. *Process Saf. Environ. Prot.* **2026**, *208*, 108471. [CrossRef]
9. Han, C.; Chen, Z. Durability Study of Gas Diffusion Backing in Proton Exchange Membrane Fuel Cells under Reverse Current Conditions. *J. Power Sources* **2024**, *603*, 234414. [CrossRef]
10. Han, C.; Jiang, T.; Shang, K.; Xu, B.; Chen, Z. Heat and Mass Transfer Performance of Proton Exchange Membrane Fuel Cells with Electrode of Anisotropic Thermal Conductivity. *Int. J. Heat Mass Transf.* **2022**, *182*, 121957. [CrossRef]
11. Giner-Sanz, J.J.; Ortega, E.M.; Pérez-Herranz, V. Mechanistic Equivalent Circuit Modelling of a Commercial Polymer Electrolyte Membrane Fuel Cell. *J. Power Sources* **2018**, *379*, 328–337. [CrossRef]
12. Busquet, S.; Hubert, C.E.; Labbé, J.; Mayer, D.; Metkemeijer, R. A New Approach to Empirical Electrical Modelling of a Fuel Cell, an Electrolyser or a Regenerative Fuel Cell. *J. Power Sources* **2004**, *134*, 41–48. [CrossRef]
13. Han, J.; Han, J.; Ji, H.; Yu, S. "Model-Based" Design of Thermal Management System of a Fuel Cell "Air-Independent" Propulsion System for Underwater Shipboard. *Int. J. Hydrogen Energy* **2020**, *45*, 32449–32463. [CrossRef]
14. Amphlett, J.C.; Baumert, R.M.; Mann, R.F.; Peppley, B.A.; Roberge, P.R.; Harris, T.J. Performance Modeling of the Ballard Mark IV Solid Polymer Electrolyte Fuel Cell: II. Empirical Model Development. *J. Electrochem. Soc.* **1995**, *142*, 9–15. [CrossRef]

15. Abdel-Basset, M.; Mohamed, R.; Elhoseny, M.; Chakrabortty, R.K.; Ryan, M.J. An Efficient Heap-Based Optimization Algorithm for Parameters Identification of Proton Exchange Membrane Fuel Cells Model: Analysis and Case Studies. *Int. J. Hydrogen Energy* **2021**, *46*, 11908–11925. [CrossRef]
16. El-Fergany, A.A. Extracting Optimal Parameters of PEM Fuel Cells Using Salp Swarm Optimizer. *Renew. Energy* **2018**, *119*, 641–648. [CrossRef]
17. Zhang, G.; Xiao, C.; Razmjooy, N. Optimal Parameter Extraction of PEM Fuel Cells by Meta-Heuristics. *Int. J. Ambient Energy* **2022**, *43*, 2510–2519. [CrossRef]
18. Sultan, H.M.; Menesy, A.S.; Kamel, S.; Tostado-Véliz, M.; Jurado, F. Parameter Identification of Proton Exchange Membrane Fuel Cell Stacks Using Bonobo Optimizer. In *Proceedings of the 2020 IEEE International Conference on Environment and Electrical Engineering and 2020 IEEE Industrial and Commercial Power Systems Europe (EEEIC/I&CPS Europe), Madrid, Spain, 9–12 June 2020*; IEEE: New York, NY, USA, 2020; pp. 1–7.
19. Kamel, S.; Jurado, F.; Sultan, H.; Menesy, A. Tree Growth Algorithm for Parameter Identification of Proton Exchange Membrane Fuel Cell Models. *Int. J. Interact. Multimed. Artif. Intell.* **2020**, *6*, 101–111.
20. Yang, F.; Li, Y.; Chen, D.; Hu, S.; Xu, X. Parameter Identification of PEMFC Steady-State Model Based on p-Dimensional Extremum Seeking via Simplex Tuning Optimization Method. *Energy* **2024**, *292*, 130601. [CrossRef]
21. Fathy, A.; Rezk, H. Multi-Verse Optimizer for Identifying the Optimal Parameters of PEMFC Model. *Energy* **2018**, *143*, 634–644. [CrossRef]
22. Ashraf, H.; Abdellatif, S.O.; Elkholy, M.M.; El-Fergany, A.A. Computational Techniques Based on Artificial Intelligence for Extracting Optimal Parameters of PEMFCs: Survey and Insights. *Arch. Comput. Methods Eng.* **2022**, *29*, 3943–3972. [CrossRef]
23. Rao, Y.; Shao, Z.; Ahangarnejad, A.H.; Gholamalizadeh, E.; Sobhani, B. Shark Smell Optimizer Applied to Identify the Optimal Parameters of the Proton Exchange Membrane Fuel Cell Model. *Energy Convers. Manag.* **2019**, *182*, 1–8. [CrossRef]
24. Askarzadeh, A.; Rezazadeh, A. A New Heuristic Optimization Algorithm for Modeling of Proton Exchange Membrane Fuel Cell: Bird Mating Optimizer. *Int. J. Energy Res.* **2013**, *37*, 1196–1204. [CrossRef]
25. Ye, M.; Wang, X.; Xu, Y. Parameter Identification for Proton Exchange Membrane Fuel Cell Model Using Particle Swarm Optimization. *Int. J. Hydrogen Energy* **2009**, *34*, 981–989. [CrossRef]
26. Rizk-Allah, R.M.; El-Fergany, A.A. Artificial Ecosystem Optimizer for Parameters Identification of Proton Exchange Membrane Fuel Cells Model. *Int. J. Hydrogen Energy* **2021**, *46*, 37612–37627. [CrossRef]
27. Fathy, A.; Elaziz, M.A.; Alharbi, A.G. A Novel Approach Based on Hybrid Vortex Search Algorithm and Differential Evolution for Identifying the Optimal Parameters of PEM Fuel Cell. *Renew. Energy* **2020**, *146*, 1833–1845. [CrossRef]
28. Turgut, O.E.; Coban, M.T. Optimal Proton Exchange Membrane Fuel Cell Modelling Based on Hybrid Teaching Learning Based Optimization—Differential Evolution Algorithm. *Ain Shams Eng. J.* **2016**, *7*, 347–360. [CrossRef]
29. Mei, J.; Meng, X.; Tang, X.; Li, H.; Hasanien, H.; Alharbi, M.; Dong, Z.; Shen, J.; Sun, C.; Fan, F.; et al. An Accurate Parameter Estimation Method of the Voltage Model for Proton Exchange Membrane Fuel Cells. *Energies* **2024**, *17*, 2917. [CrossRef]
30. Alqahtani, A.H.; Hasanien, H.M.; Alharbi, M.; Chuanyu, S. Parameters Estimation of Proton Exchange Membrane Fuel Cell Model Based on an Improved Walrus Optimization Algorithm. *IEEE Access* **2024**, *12*, 74979–74992. [CrossRef]
31. Abdollahzadeh, B.; Khodadadi, N.; Barshandeh, S.; Trojovský, P.; Gharehchopogh, F.S.; El-kenawy, E.S.M.; Abualigah, L.; Mirjalili, S. *Puma Optimizer (PO): A Novel Metaheuristic Optimization Algorithm and Its Application in Machine Learning*; Springer: Berlin/Heidelberg, Germany, 2024; Volume 5.
32. Kanouni, B.; Laib, A. Extracting Accurate Parameters from a Proton Exchange Membrane Fuel Cell Model Using the Differential Evolution Ameliorated Meta-Heuristics Algorithm. *Energies* **2024**, *17*, 2333. [CrossRef]
33. Mann, R.F.; Amphlett, J.C.; Hooper, M.A.I.; Jensen, H.M.; Peppley, B.A.; Roberge, P.R. Development and Application of a Generalised Steady-State Electrochemical Model for a PEM Fuel Cell. *J. Power Sources* **2000**, *86*, 173–180. [CrossRef]
34. Zhang, G.; Jiao, K. Three-Dimensional Multi-Phase Simulation of PEMFC at High Current Density Utilizing Eulerian-Eulerian Model and Two-Fluid Model. *Energy Convers. Manag.* **2018**, *176*, 409–421. [CrossRef]
35. Kanouni, B.; Laib, A.; Necaibia, S.; Krama, A.; Guerrero, J.M. Circulatory System-Based Optimization: A Biologically Inspired Metaheuristic Approach for Accurately Identifying a PEMFC's Parameters. *Energy Rep.* **2025**, *13*, 4661–4677. [CrossRef]
36. Ashraf, H.; Abdellatif, S.O.; Elkholy, M.M.; El-Fergany, A.A. Honey Badger Optimizer for Extracting the Ungiven Parameters of PEMFC Model: Steady-State Assessment. *Energy Convers. Manag.* **2022**, *258*, 115521. [CrossRef]
37. Bilal; Pant, M.; Zaheer, H.; Garcia-Hernandez, L.; Abraham, A. Differential Evolution: A Review of More than Two Decades of Research. *Eng. Appl. Artif. Intell.* **2020**, *90*, 103479. [CrossRef]
38. Sultan, H.M.; Menesy, A.S.; Korashy, A.; Hussien, A.G.; Kamel, S. Enhancing Parameter Identification for Proton Exchange Membrane Fuel Cell Using Modified Manta Ray Foraging Optimization. *Energy Rep.* **2024**, *12*, 1987–2013. [CrossRef]
39. Priya, K.; Selvaraj, V.; Ramachandra, N.; Rajasekar, N. Modelling of PEM Fuel Cell for Parameter Estimation Utilizing Clan Co-Operative Based Spotted Hyena Optimizer. *Energy Convers. Manag.* **2024**, *309*, 118371. [CrossRef]

40. Sultan, H.M.; Menesy, A.S.; Kamel, S.; Selim, A.; Jurado, F. Parameter Identification of Proton Exchange Membrane Fuel Cells Using an Improved Salp Swarm Algorithm. *Energy Convers. Manag.* **2020**, *224*, 113341. [CrossRef]
41. Kanouni, B.; Laib, A.; Necaibia, S.; Krama, A.; Guerrero, J.M. Pied Kingfisher Optimizer for Accurate Parameter Extraction in Proton Exchange Membrane Fuel Cell. *Energy* **2025**, *325*, 136079. [CrossRef]
42. Menesy, A.S.; Sultan, H.M.; Korashy, A.; Banakhr, F.A.; Ashmawy, M.G.; Kamel, S. Effective Parameter Extraction of Different Polymer Electrolyte Membrane Fuel Cell Stack Models Using a Modified Artificial Ecosystem Optimization Algorithm. *IEEE Access* **2020**, *8*, 31892–31909. [CrossRef]
43. Menesy, A.S.; Sultan, H.M.; Selim, A.; Ashmawy, M.G.; Kamel, S. Developing and Applying Chaotic Harris Hawks Optimization Technique for Extracting Parameters of Several Proton Exchange Membrane Fuel Cell Stacks. *IEEE Access* **2020**, *8*, 1146–1159. [CrossRef]
44. Ferahtia, S.; Houari, A.; Rezk, H.; Djerioui, A.; Machmoum, M.; Motahhir, S.; Ait-Ahmed, M. *Red-Tailed Hawk Algorithm for Numerical Optimization and Real-World Problems*; Nature Publishing Group: London, UK, 2023; Volume 13.
45. El-Fergany, A.A.; Hasanien, H.M.; Agwa, A.M. Semi-Empirical PEM Fuel Cells Model Using Whale Optimization Algorithm. *Energy Convers. Manag.* **2019**, *201*, 112197. [CrossRef]
46. Tang, X.; Yang, M.; Shi, L.; Hou, Z.; Xu, S.; Sun, C. Adaptive State-of-Health Temperature Sensitivity Characteristics for Durability Improvement of PEM Fuel Cells. *Chem. Eng. J.* **2024**, *491*, 151951. [CrossRef]
47. Meng, X.; Liu, M.; Mei, J.; Li, X.; Grigoriev, S.; Hasanien, H.M.; Tang, X.; Li, R.; Sun, C. Polarization Loss Decomposition-Based Online Health State Estimation for Proton Exchange Membrane Fuel Cells. *Int. J. Hydrogen Energy* **2025**, *157*, 150162. [CrossRef]